Performance of an Iterative Multi-User Receiver for MIMO-OFDM Systems in a Real Indoor Scenario

Salvo Rossi, Pierluigi; Hammarberg, Peter; Tufvesson, Fredrik; Edfors, Ove; Almers, Peter; Kolmonen, Veli-Matti; Koivunen, Jukka; Haneda, Hatsuyuki; Muller, Ralf

Published in:
[Host publication title missing]

DOI:
10.1109/GLOCOM.2008.ECP.857

2008

Performance of an Iterative Multi-User Receiver for MIMO-OFDM Systems in a Real Indoor Scenario

P. Salvo Rossi*, P. Hammarberg†, F. Tufvesson†, O. Edfors†, P. Almers†,
V.-M. Kolmonen‡, J. Koivunen‡, K. Haneda‡. R.R. Müller*

*Dept. of Electronics and Telecommunications, Norwegian University of Science and Technology, Trondheim, Norway.
†Department of Electrical and Information Technology, Lund University, Lund, Sweden.
‡Radio Laboratory, Helsinki University of Technology, Helsinki, Finland.

***Abstract*—This paper aims at validation of an iterative receiver for Multiple-Input Multiple-Output with Orthogonal Frequency Division Multiplexing (MIMO-OFDM) systems using real-measurement channel data from an indoor scenario. The receiver performs iterative Multi-User Detection (MUD) and Channel Estimation (CE) via soft information from the single-user decoders. The Channel measurements were performed for a dynamic dual MIMO link scenario. The case with two users with multiple antennas interfering each other is considered. CE at the receiver exploits the frequency correlation of the MIMO link. Simulation results for the performance are shown in terms of Bit-Error Rate (BER) vs. Signal-to-Noise Ratio (SNR). Performance for the whole system are provided and compared with respect to the case of Perfect Channel-State Information (PCSI) at the receiver, as well as for the single user. We also provide an analysis of BER with respect to Signal-to-Interference Ratio (SIR). CE performance are evaluated in terms of Normalized Mean Square Error (NMSE).**

I. Introduction

Multiple-Input Multiple-Output (MIMO) systems in combination with Orthogonal Frequency Division Multiplexing (OFDM) and iterative receivers have gained interest in current research in wireless communications. MIMO-OFDM systems simultaneously mitigate inter-symbol interference and enhance system capacity [1], while iterative receivers, using Multi-User Detection (MUD) and Channel Estimation (CE), can achieve near-optimum performance with reasonable complexity [2].

In this paper we test an iterative receiver for MIMO-OFDM systems on unique channel measurements from a real indoor dual-link scenario assuming a "quasi-static" channel, i.e. block-fading. The receiver is similar to the one presented in [3], with the time-variant channel estimator replaced with a different estimator exploiting both frequency correlation and block-fading assumption. Compared to a computer-simulated channel, the real-world channel shows a higher variability on received power, thus a highly varying Signal-to-Noise Ratio (SNR). Performance are analyzed in terms of Bit-Error Rate (BER) vs. SNR. The impact of the iterations for both the system performance and the single user performance is analyzed, and the case of Perfect Channel-State Information (PCSI) at the receiver is used as reference. Performance of CE are evaluated via Normalized Mean Square Error (NMSE).

[0]This work has been supported by the Research Council of Norway (NFR), by the Swedish Governmental Agency for Innovation Systems (VINNOVA), and by Finnish Funding Agency for Technology and Innovation (TEKES), under the project WILATI within the NORDITE framework.

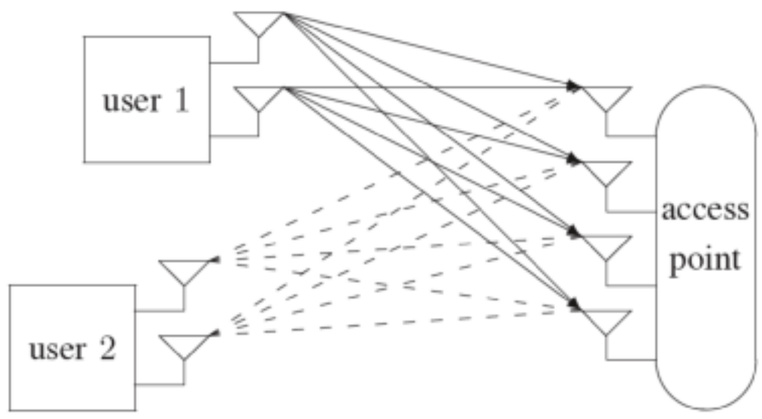

Fig. 1. Considered scenario.

Finally, a preliminary analysis of the performance with respect to Signal-to-Interference Ratio (SIR) between the two users is performed.

The paper is organized as follows: the mathematical model for the considered MIMO-OFDM system and the structure of the iterative receiver are described in Section II; in Section III we describe the data representing the real channels used for validation of the receiver; Section IV shows, compares, and analyzes the performance of the receiver obtained via numerical simulations; some concluding remarks are given in Section V.

Notation - Column vectors (resp. matrices) are denoted with lower-case (resp. upper-case) bold letters; a_i (resp. $A_{i,j}$) denotes the ith (resp. (i,j)th) element of vector $\boldsymbol{a}$ (resp. matrix $\boldsymbol{A}$); $\mathrm{diag}(\boldsymbol{a})$ denotes a diagonal matrix whose main diagonal is $\boldsymbol{a}$. $\boldsymbol{I}_N$ denotes the $N \times N$ identity matrix; $\boldsymbol{i}_N^{(n)}$ denotes the nth column of $\boldsymbol{I}_N$; $\boldsymbol{e}_N$ denotes a vector of length N whose elements are 1; $\mathbb{E}\{.\}$, $(.)^*$, $(.)^{\mathrm{T}}$ and $(.)^{\mathrm{H}}$ denote expectation, conjugate, transpose and conjugate transpose operators; $\delta_{i,j}$ is the Kronecker delta; $\otimes$ denotes the Kronecker matrix product; $\Re(a)$ and $\Im(a)$ denote the real and imaginary parts of a; $\lceil a \rceil$ denotes the smallest integer value greater than or equal to a; j denotes the imaginary unit; $\mathcal{N}(\mu, \sigma^2)$ denotes the normal distribution with mean μ and variance σ^2; $\mathcal{N}_{\mathbb{C}}(\boldsymbol{\mu}, \boldsymbol{\Sigma})$ denotes the circular symmetric complex normal distribution with mean vector $\boldsymbol{\mu}$ and covariance matrix $\boldsymbol{\Sigma}$; the symbol $\sim$ means "distributed as".

II. System Model

We consider a MIMO-OFDM system with K transmit antennas and N receive antennas in which each transmit antenna sends an independent data stream. Each stream is encoded via convolutional coding and random interleaving, with codewords spanning both time and frequency dimensions. Transmission is frame oriented: a frame is composed of S OFDM symbols each with M subcarriers. Pilots for CE at the receiver are allocated into S_p OFDM symbols, while the remaining $S - S_p$ OFDM symbols are left for conveying one single codeword. Quadrature Phase Shift Keying (QPSK) modulation is considered [4], thus each frame consists of $L = 2MS$ bits, of which $2MS_p$ are pilot bits and $2M(S-S_p)$ are code bits.

In the following, for the generic frame: $b_k[\ell]$ and $c_k[\ell]$ denote the ℓth source bit and the ℓth code bit (including pilots) to be transmitted by the kth transmit antenna; $x_k[m,s]$ denotes the QPSK symbol transmitted by the kth transmit antenna on the mth subcarrier during transmission of the sth OFDM symbol; $H_{n,k}[m]$ denotes the channel coefficient between the kth transmit antenna and the nth receive antenna on the mth subcarrier during transmission of all the S OFDM symbols in the frame; $w_n[m,s]$ denotes the additive noise at the nth receive antenna on the mth subcarrier during transmission of the sth OFDM symbol; $r_n[m,s]$ denotes the received signal at the nth receive antenna on the mth subcarrier during transmission of the sth OFDM symbol. Referring to the mth subcarrier during transmission of the sth OFDM symbol, we denote transmitted vector, channel matrix, AWGN vector, and received vector as

$$\begin{aligned}
\boldsymbol{x}[m,s] &= (x_1[m,s],\ldots,x_K[m,s])^{\mathrm{T}} \\
\boldsymbol{H}[m] &= \begin{pmatrix} H_{1,1}[m] & \ldots & H_{1,K}[m] \\ \vdots & \ddots & \vdots \\ H_{N,1}[m] & \ldots & H_{N,K}[m] \end{pmatrix}, \\
\boldsymbol{w}[m,s] &= (w_1[m,s],\ldots,w_N[m,s])^{\mathrm{T}}, \\
\boldsymbol{r}[m,s] &= (r_1[m,s],\ldots,r_N[m,s])^{\mathrm{T}}.
\end{aligned}$$

The channel vector from the kth transmit antenna is $\boldsymbol{h}_k^{(\mathrm{tx})}[m] = \boldsymbol{H}[m]\boldsymbol{i}_K^{(k)}$. The discrete-time model for the received signal is

$$\boldsymbol{r}[m,s] = \boldsymbol{H}[m]\boldsymbol{x}[m,s] + \boldsymbol{w}[m,s]\ . \tag{1}$$

QPSK mapping (from bits to QPSK symbols) is based on

$$x_k[m,s] = \frac{1}{\sqrt{2}}\left(c_k(2\ell-1) - jc_k(2\ell)\right)\ ,$$

while QPSK demapping (from QPSK symbols to bits) on

$$\begin{cases} c_k(2\ell-1) = \Re(x_k[m,s]) \\ c_k(2\ell) = -\Im(x_k[m,s]) \end{cases},$$

where $\ell = (s-1)M + m$.

OFDM symbols are demodulated and sent to the iterative decoder performing MUD, Soft-Input Soft-Output (SISO) decoding and CE. The multiuser detector and SISO decoders exchange extrinsic information on symbols x_k, denoted $\tilde{x}_k$ when fed to the multiuser detector and $\tilde{z}_k$ when fed to the SISO decoders. SISO decoders also provide *a posteriori* information on symbol x_k, denoted $\hat{x}_k$, to the channel estimator, and *a posteriori* information on source bits. The channel estimator provides estimates for the channel coefficients ($\hat{H}_{n,k}$). Perfect synchronization between users is assumed, which is valid as long as synchronization errors do not exceed the length of the cyclic prefix.

It is worth noticing that SISO decoders pre-process $\{\tilde{z}_k[1],\ldots,\tilde{z}_k[L_x]\}$ via demapping and deinterleaving, and post-process $\{\tilde{x}_k[1],\ldots,\tilde{x}_k[L_x]\}$ and $\{\hat{x}_k[1],\ldots,\hat{x}_k[L_x]\}$ via interleaving and mapping.

A. MUD

The received signals (1) are processed separately for each subcarrier and OFDM symbol. Parallel interference cancellation is performed using $\tilde{\boldsymbol{x}}$ from the SISO decoders and $\hat{\boldsymbol{H}}$ from the channel estimators. The residual term from the interference cancellation for the kth transmit antennas, $\tilde{\boldsymbol{r}}_{(k)} = \boldsymbol{r} - \hat{\boldsymbol{H}}(\tilde{\boldsymbol{x}} - \tilde{x}_k\boldsymbol{i}_K^{(k)})$, is then MMSE filtered, to reduce noise and multiaccess interference, giving the extrinsic information

$$\tilde{z}_k = \frac{\boldsymbol{i}_K^{(k)\mathrm{T}}\left(\hat{\boldsymbol{H}}^{\mathrm{H}}\hat{\boldsymbol{H}} + \sigma_w^2\boldsymbol{V}_{(k)}^{-1}\right)^{-1}\hat{\boldsymbol{H}}^{\mathrm{H}}\tilde{\boldsymbol{r}}_{(k)}}{\boldsymbol{i}_K^{(k)\mathrm{T}}\left(\hat{\boldsymbol{H}}^{\mathrm{H}}\hat{\boldsymbol{H}} + \sigma_w^2\boldsymbol{V}_{(k)}^{-1}\right)^{-1}\hat{\boldsymbol{H}}^{\mathrm{H}}\hat{\boldsymbol{h}}_{(k)}}\ ,$$

with $\boldsymbol{V}_{(k)} = \mathrm{diag}\left((1-|\tilde{x}_1|^2,\ldots,1-|\tilde{x}_{k-1}|^2,1,1-|\tilde{x}_{k+1}|^2,\ldots,1-|\tilde{x}_K|^2)\right)$. For the derivation we refer to [3].

B. SISO Decoding

After collecting $\{\tilde{z}_k[\ell]\}_{\ell=1}^{L}$, each transmit antenna can be decoded independently using the log-domain BCJR algorithm [5], [6]. The SISO decoder for the kth transmit antenna utilizes the model [7] $\tilde{z}_k = \mu_k x_k + v_k$, with $v_k \sim \mathcal{N}_{\mathbb{C}}(0,\eta_k^2)$, where $\mu_k = 1$, and $\eta_k^2 = \left(\boldsymbol{i}_K^{(k)\mathrm{T}}\left(\boldsymbol{H}^{\mathrm{H}}\boldsymbol{H} + \sigma_w^2\boldsymbol{I}_N\right)^{-1}\boldsymbol{H}^{\mathrm{H}}\boldsymbol{h}_{(k)}\right)^{-1}$.

C. CE

Assuming that the maximum normalized delay spread ($\eta_{\max}^{(\mathrm{d})}$) is known, the receiver implements a low-complexity estimator based on the following Slepian expansion

$$H_{n,k}[m] \approx \sum_{i=1}^{I}\psi_{n,k}[i]v_i[m]\ ,$$

where $\psi_{n,k}[i]$ is the ith Slepian coefficient for the link between the kth transmit antenna and the nth receive antenna; $v_i[m]$ is the mth sample of the ith time-shifted DPS sequence associated to the interval $m = 1,\ldots,M$ with time support $[0,\eta_{\max}^{(\mathrm{d})}]$ with corresponding eigenvalue $\lambda_i^{(\mathrm{d})}$; the approximate signal space extension is $\left\lceil \eta_{\max}^{(\mathrm{d})}M \right\rceil + 1 \le I \le M$, see [8] for more details. Also, we denote

$$\begin{aligned}
\boldsymbol{v}[m] &= (v_1[m],\ldots,v_I[m])^{\mathrm{T}}\ , \\
\boldsymbol{\lambda}^{(\mathrm{d})} &= \left(\lambda_1^{(\mathrm{d})},\ldots,\lambda_I^{(\mathrm{d})}\right)^{\mathrm{T}}\ , \\
\boldsymbol{\Xi}[m,s] &= \boldsymbol{I}_N \otimes (\boldsymbol{x}[m,s]\otimes\boldsymbol{v}[m])^{\mathrm{T}}\ , \\
\boldsymbol{\psi}_{n,k} &= (\psi_{n,k}[1],\ldots,\psi_{n,k}[I])^{\mathrm{T}}\ ,
\end{aligned}$$

The signal model for CE is

$$\boldsymbol{r} = \boldsymbol{\Xi}\boldsymbol{\psi} + \boldsymbol{w} \,,$$

with $\boldsymbol{r}$, $\boldsymbol{\Xi}$, $\boldsymbol{\psi}$ and $\boldsymbol{w}$ appropriately collecting received signals, transmitted signals, Slepian coefficients and noise, as follows:

$$\begin{aligned}
\boldsymbol{r} &= \left(\boldsymbol{r}^{\mathrm{T}}[1], \ldots, \boldsymbol{r}^{\mathrm{T}}[S]\right)^{\mathrm{T}} \,, \\
\boldsymbol{r}[s] &= \left(\boldsymbol{r}^{\mathrm{T}}[1,s] \ldots, \boldsymbol{r}^{\mathrm{T}}[M,s]\right)^{\mathrm{T}} \,, \\
\boldsymbol{\Xi} &= \left(\boldsymbol{\Xi}^{\mathrm{T}}[1], \ldots, \boldsymbol{\Xi}^{\mathrm{T}}[S]\right)^{\mathrm{T}} \,, \\
\boldsymbol{\Xi}[s] &= \left(\boldsymbol{\Xi}^{\mathrm{T}}[1,s], \ldots, \boldsymbol{\Xi}^{\mathrm{T}}[M,s]\right)^{\mathrm{T}} \,, \\
\boldsymbol{w} &= \left(\boldsymbol{w}^{\mathrm{T}}[1], \ldots, \boldsymbol{w}^{\mathrm{T}}[S]\right)^{\mathrm{T}} \,, \\
\boldsymbol{w}[s] &= \left(\boldsymbol{w}^{\mathrm{T}}[1,s], \ldots, \boldsymbol{w}^{\mathrm{T}}[M,s]\right)^{\mathrm{T}} \,, \\
\boldsymbol{\psi} &= \left(\boldsymbol{\psi}_1^{\mathrm{T}}, \ldots, \boldsymbol{\psi}_N^{\mathrm{T}}\right)^{\mathrm{T}} \,, \\
\boldsymbol{\psi}_n &= \left(\boldsymbol{\psi}_{n,1}^{\mathrm{T}}, \ldots, \boldsymbol{\psi}_{n,K}^{\mathrm{T}}\right)^{\mathrm{T}} \,.
\end{aligned}$$

A linear MMSE estimate is performed

$$\hat{\boldsymbol{\psi}} = \left(\hat{\boldsymbol{\Xi}}^{\mathrm{H}} \boldsymbol{\Delta}^{-1} \hat{\boldsymbol{\Xi}} + \boldsymbol{C}_{\psi}^{-1}\right)^{-1} \hat{\boldsymbol{\Xi}}^{\mathrm{H}} \boldsymbol{\Delta}^{-1} \boldsymbol{r} \,,$$

where $\boldsymbol{C}_{\psi} = \frac{1}{\eta_{\max}^{(\mathrm{d})}} \boldsymbol{I}_{NK} \otimes \mathrm{diag}\left(\boldsymbol{\lambda}^{(\mathrm{d})}\right)$ denotes the covariance matrix of the Slepian coefficients; $\hat{\boldsymbol{\Xi}}$ contains the expected transmitted symbols computed via *a posteriori* information from SISO decoders; $\boldsymbol{\Delta} = \boldsymbol{\Theta} + \sigma_w^2 \boldsymbol{I}_{NMS}$, being

$$\begin{aligned}
\boldsymbol{\Theta} &= \mathrm{diag}(\boldsymbol{\vartheta}) \,, \\
\boldsymbol{\vartheta} &= \left(\boldsymbol{\vartheta}^{\mathrm{T}}[1], \ldots, \boldsymbol{\vartheta}^{\mathrm{T}}[S]\right)^{\mathrm{T}} \,, \\
\boldsymbol{\vartheta}[s] &= \left(\boldsymbol{\vartheta}^{\mathrm{T}}[1,s], \ldots, \boldsymbol{\vartheta}^{\mathrm{T}}[M,s]\right)^{\mathrm{T}} \,, \\
\boldsymbol{\vartheta}[m,s] &= \left(\sum_{k=1}^{K} \left(1 - |\hat{x}_k[m,s]|^2\right)\right) \boldsymbol{e}_N \,.
\end{aligned}$$

NMSE for CE performance evaluation is computed as

$$\mathrm{NMSE}_{\mathrm{H}} = \frac{\mathbb{E}\{|H_{n,k}[m] - \hat{H}_{n,k}[m]|^2\}}{\mathbb{E}\{|H_{n,k}[m]|^2\}} \,.$$

III. The Channel Measurement Data

The performance of the receiver is analyzed using *measured dynamic dual-link* MIMO channels. Post-processing of the channel measurements was needed due to the presence of measurement noise and due to the spacing of the frequency sampling points. Sections III-A and III-B describe the measurements and the post-processing, respectively.

A. Dynamic Multi-link MIMO Channel Measurements

The measurements were carried out in September 2007 in the CS-building of *Helsinki University of Technology*, Helsinki, Finland. The building is a modern four storage building with corridors and offices surrounding a large atrium in the middle, resembling an airport terminal or a shopping mall. The measurements were performed using a mobile transmitter and two different stationary receivers. The measurement scenario may be seen as a real-life application with two users, transmitting to one access point.

TABLE I
Measurement parameters.

Center frequency	5.3 GHz
Bandwidth	120 MHz
TX power	0.5 W (27 dBm)
Gap between MIMO blocks	39.3216 ms

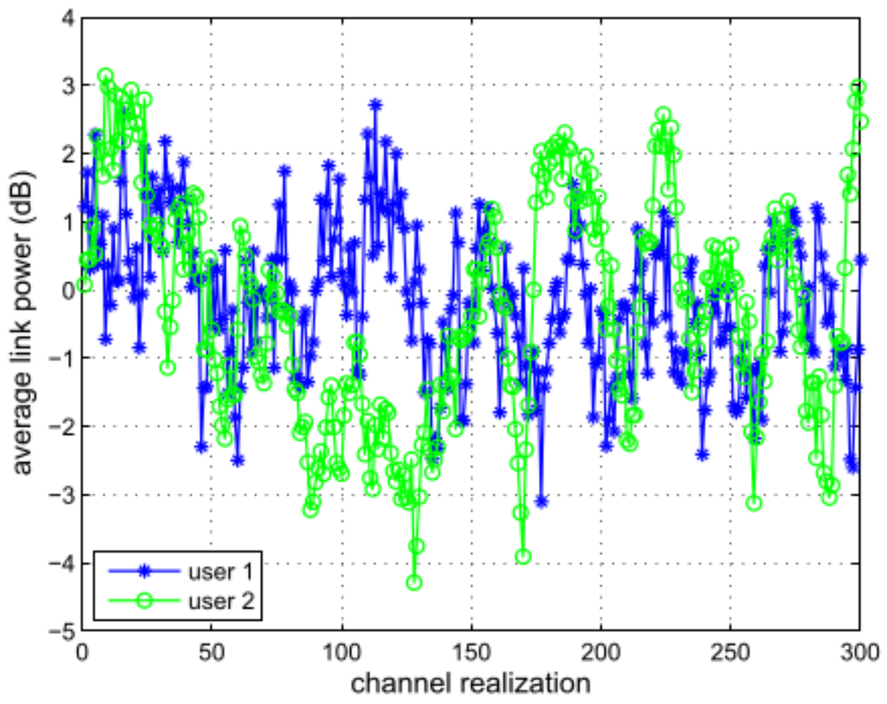

Fig. 2. Average power for the two links.

The measurement setup is summarized here (for a more detailed description refer to [9]) and some measurement parameters can be found in Table I. In order to capture the variation of the multi-link MIMO scenario, a single signal was transmitted from the transmitter to both of the two receivers. The transmitter was moved along several routes with a speed of about 1 m/s. The MIMO channel transfer function was sampled each 39 ms. Due to the short frame time in typical applications and low expected speed of movements, the channel is approximately constant over several frames. Local rubidium clocks in the sounders were used for synchronization. In the simulations each sample represents an independent channel realization. Sixteen dual-polarized antennas were used at each link end.

The resulting data files from the measurements include two 32×32 MIMO channels, which was reduced to two 4×2 MIMO channels which then was combined in order to provide the joint channel matrix. The MIMO channels were chosen to get a high measurement SNR, in order to reduce the effects of the measurement noise. For the analysis we have selected a scenario where the power from the two users is well balanced.

B. Processing of Channel Measurements

Data filtering has been performed in order to reduce the significant amount of measurement noise present in the channel data, allowing the measured transfer function to be used in the simulations directly. Also, interpolation has been performed in order to change the original frequency spacing in the measurements (0.6250 MHz) to a subcarrier spacing of 0.3125 MHz, in accordance with the recent IEEE 802.11n WLAN proposal [10].

The interpolation and the noise reduction were performed using an interpolating Wiener filter [11] in the frequency

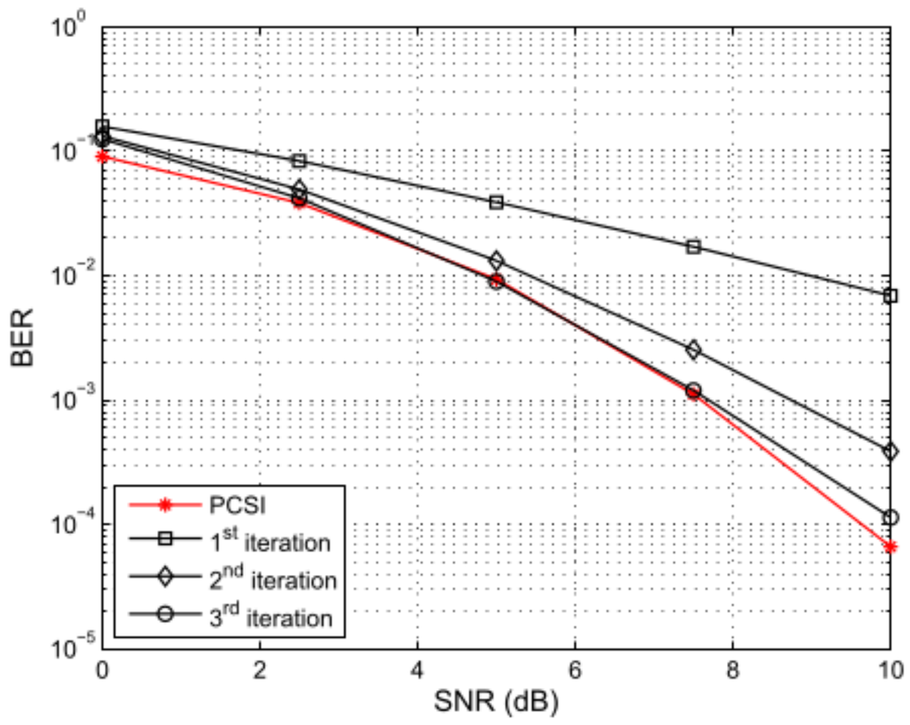

(a) BER-vs-SNR.

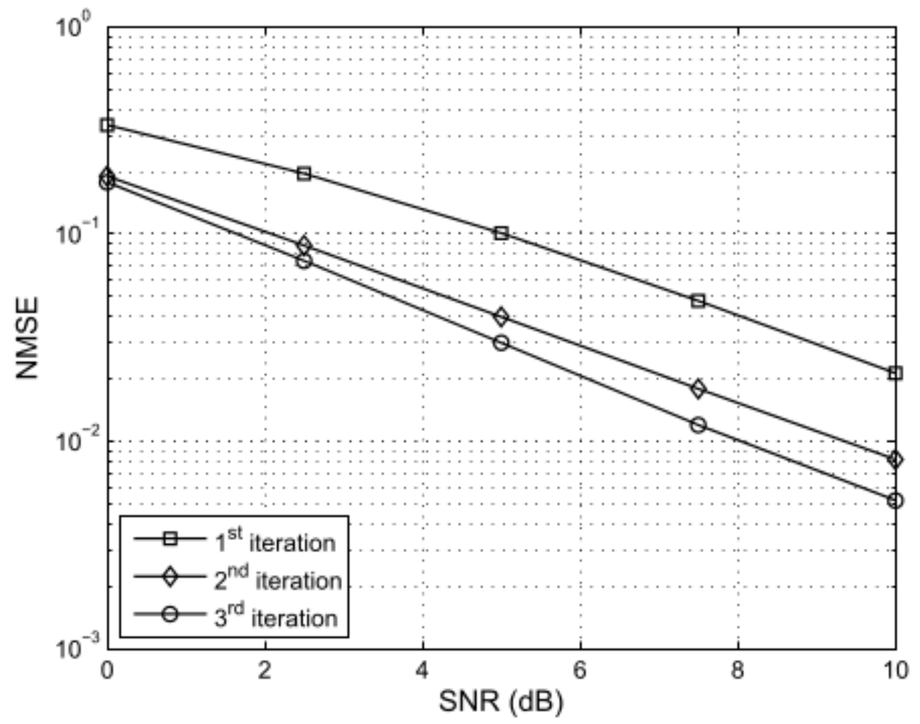

(b) NMSE-vs-SNR.

Fig. 3. Simulation results for a 4×4 system with $M = 64$ subcarriers and $S = 20$ OFDM symbols per frame including $S_p = 4$ OFDM pilot symbols.

domain. A rectangular power delay profile of length 0.2 (normalized delay) was chosen in order to get a reasonable noise reduction and still preserve the channel energy.

From the selected scenario a subset of the channel realizations were extracted for simulations and validation of the iterative receiver. The realizations were chosen in order to have small variations of the average power in the two links. Normalization was performed in order to have the same average (taken over the whole set of channel realizations) received power for both users. In Fig. 2 the average power, taken over antennas and frequency, for the links corresponding to the two users is shown. The realizations correspond to consecutive measurement points in time. It is apparent that the individual link power for the two users vary over the different channel realizations. On average the SIR is 0.6 dB in favor of user 1.

IV. Simulation Results

As mentioned above, the system under consideration consists of two users with 2 transmit antennas each and one access point with 4 receive antennas. Each transmit antenna sends independent codewords spanning $S = 20$ OFDM symbols, including $S_p = 4$ OFDM pilot symbols, and each OFDM symbols covers $M = 64$ subcarriers. The number of pilots was chosen as the minimum to achieve maximum capacity for the MIMO channel [12]. Code bits are generated at rate $1/2$ via a recursive systematic convolutional encoder [4] with generators $(7, 5)_8$ and with two tail bits used to enforce the final state into 1, thus giving 2044 information bit per frame. Assuming 4μs for transmission of one single OFDM symbol [10], each user in the considered system transmits at 26 $Mbps$. The block-fading assumption is valid as the relative Doppler is far below 1%.

The maximum normalized delay spread for the considered scenario is $\eta_{\max}^{(\mathrm{d})} = 0.15$ giving 11 coefficients as the lower bound for the approximate signal space extension. In the simulations, the number of coefficients for CE at the receiver is set to $I = 14$, i.e. we have a reduction of computational complexity of about 78% compared to $M = 64$. The receiver is assumed to perform 3 iterations.

Fig. 3 shows the average performance of the system. More specifically, Fig. 3(a) shows the BER performance at each iteration compared to the case of Perfect Channel-State Information (PCSI) at the receiver, while Fig. 3(b) shows the corresponding NMSE for the CE. It is apparent how the optimum performance, the PCSI case, are approached within a few iterations.

Also, it is interesting to notice how the iterative process reduces the difference in performance of the two users, caused by the mutual interference. The average SIR considering user 2 as the interferer is around 0.6 dB, thus user 1 experiences slightly better performance at the first iteration. However, the iterative process makes both users benefit from the interference cancellation and consequently the difference in performance is reduced. Fig. 4 shows how the difference in performance decreases from more than 2 dB at the first iteration to less than 1 dB at the third iteration, i.e. more than 1 dB reduction for the unbalance of the two users.

Theoretical analysis for the PCSI case with synthetic channel coefficients, as well as the impact of interference on user performance, may be found in [13], [14]. However, it should be noted that our results refer to real-world channels with CE performed at the receiver.

A preliminary analysis of the impact the interference has also been conducted. Neglecting the mutual interference at receiver side dramatically reduces the performance, thus joint reception and processing of interfering users is crucial. Fig. 5 shows the BER of a single user with respect to the level of SIR caused by the interfering user. For these results, a different subset of channel realizations were extracted from the chosen scenario in which large variations in the SIR are present. Again, normalization was performed in order to have equal average received power for the two users, and sets of ten realizations with small variations in SIR are extracted. BER

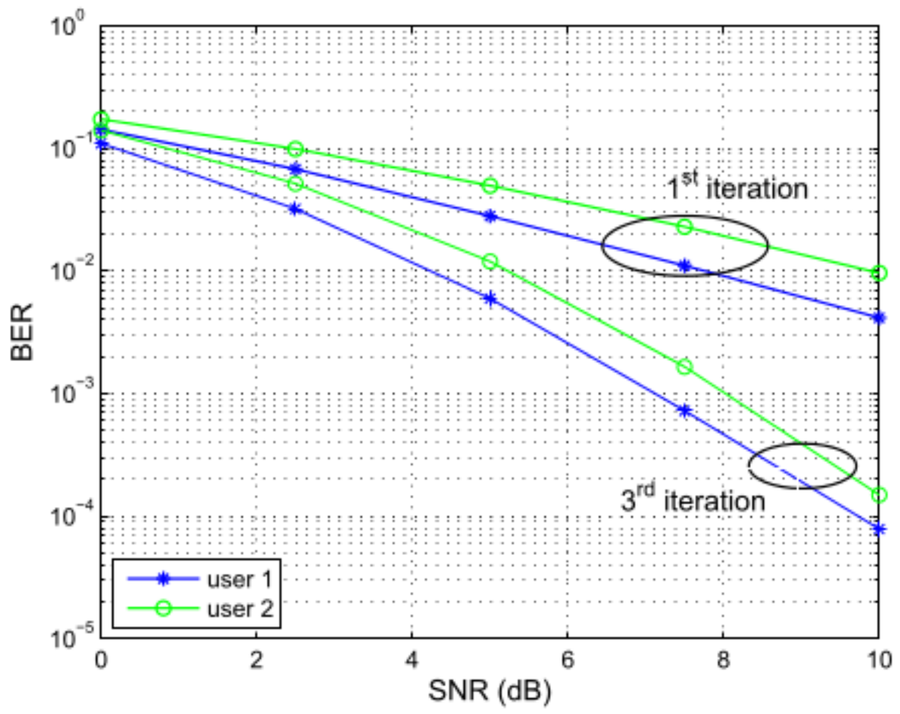

Fig. 4. Performance of the two users.

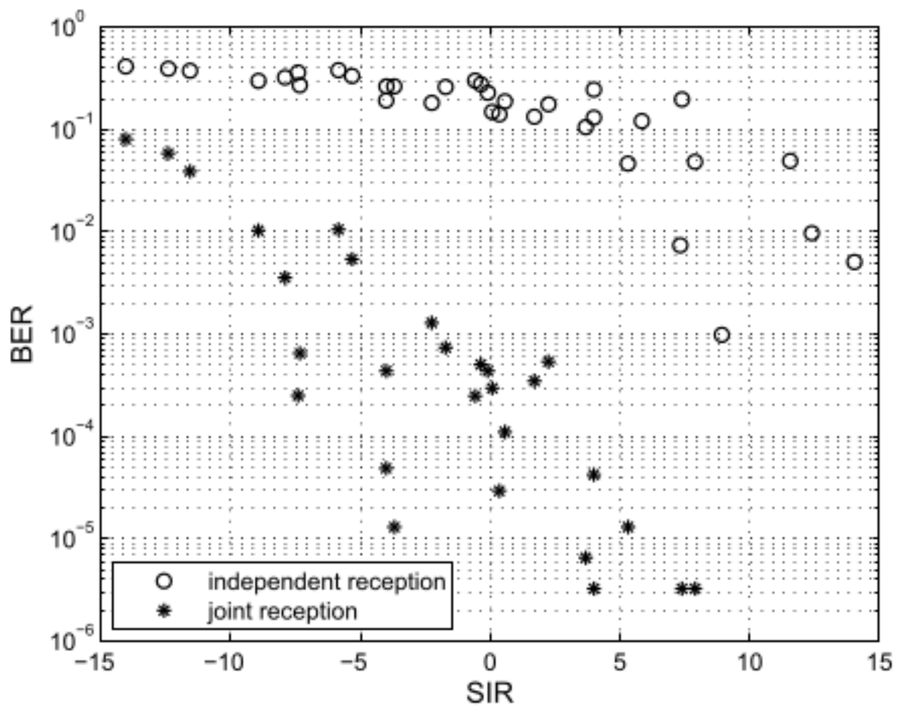

Fig. 5. SIR analysis.

has been evaluated for the various SIR cases with an SNR level of 10 dB. The average performance of the single user is evaluated for the following cases: (i) each user is received independently, neglecting the interference caused by the other user; (ii) both users are jointly received and processed. The former represents two 2×2 systems interfering each other; while the latter represents an analogous situation in which the access points are allowed to cooperate. Fig. 5 shows the performance in the two cases with respect to the level of SIR when 3 iterations are performed at the receiver. It is apparent that a big gain (about 15 dB) is achieved when joint reception and processing is allowed. Cooperation among access points is essential in order to exploit and combat multi-user interference. Again, remember though that possible synchronization errors have not been taken into account.

V. Conclusion

In this paper we have evaluated the performance of an iterative receiver performing joint MUD and CE for a system with two users with 2 antennas each and a receiver with 4 antennas. The evaluation has been performed using measured dual-link MIMO channels. Simulation results show that the iterative process reduces the BER and approaches the PCSI performance in a few iterations (3 for the given scenario). The results also show that the difference in performance of the two users, due to difference in the mutual SIR, is reduced through the iterative process.

Preliminary results for independent and joint processing at the receiver show the potential performance enhancement that can be achieved by exploiting multi-user interference. For the considered scenario the performance gain was around 15 dB.

References

[1] G.L. Stüber, J.R. Barry, S.W. McLaughlin, Y. Li, M.A. Ingram, T.G. Pratt, "Broadband MIMO-OFDM Wireless Communications," *Proceedings of the IEEE*, vol. 92, no. 2, pp. 271–294, February 2004.

[2] T. Zemen, C.F. Mecklenbräuker, J. Wehinger, R.R. Müller, "Iterative Joint Time-Variant Channel Estimation and Multi-User Detection for MC-CDMA," *IEEE Transactions on Wireless Communications*, vol. 5, no. 6, pp. 1469–1478, June 2006.

[3] P. Salvo Rossi, R.R. Müller, "Joint Iterative Time-Variant Channel Estimation and Multi-User Detection for MIMO-OFDM Systems," *IEEE Global Telecommunications Conference (GLOBECOM)*, pp. 4263–4268, November 2007.

[4] J.G. Proakis, *Digital Communications*, McGraw Hill, 2000.

[5] L.R. Bahl, J. Cocke, F. Jelinek, J. Raviv, "Optimal Decoding of Linear Codes for Minimizing Symbol Error Rate," *IEEE Transactions on Information Theory*, vol. 20, no. 2, pp. 284–287, March 1974.

[6] P. Robertson, E. Villebrun, E. Höher, "A Comparison of Optimal and Sub-Optimal MAP Decoding Algorithms Operating in the Log Domain," *IEEE International Conference on Communications (ICC)*, pp. 1009–1013, June 1995.

[7] X. Wang, H.V. Poor, "Iterative (Turbo) Soft Interference Cancellation and Decoding for Coded CDMA," *IEEE Transactions on Communications*, vol. 47, no. 7, pp. 1046–1061, July 1999.

[8] D. Slepian, "Prolate Spheroidal Wave Functions, Fourier Analysis, and Uncertainty - V: The Discrete Case," *Bell System Technical Journal*, vol. 57, no. 5, pp. 1371–1430, May/June 1978.

[9] J. Koivunen, P. Almers, V.-M. Kolmonen, J. Salmi, A. Richter, F. Tufvesson, P. Suvikunnas, A.F. Molisch, P. Vainikainen, "Dynamic multi-link indoor MIMO measurements at 5.3 GHz," *European Conference on Antennas and Propagation (EuCAP)*, November 2007.

[10] S. Coffey, A. Kasher, A. Stephens, "Joint Proposal: High Throughput Extension to the 802.11 Standard: PHY," *IEEE 802.11-05/1102r2*, January 2006.

[11] S.M. Kay, *Fundamentals of Statistical Signal Processing: Estimation Theory*, Prentice Hall, 1993.

[12] B. Hassibi, B.M. Hochwald, "How Much Training is Needed in Multiple-Antenna Wireless Links?," *IEEE Transactions on Information Theory*, vol. 49, no. 4, pp. 951–963, April 2003.

[13] H. Dai, A.F. Molisch, H.V. Poor, "Downlink Capacity of Interference-Limited MIMO Systems with Joint Detection," *IEEE Transactions on Wireless Communications*, vol. 3, no. 2, pp. 442–453, March 2004.

[14] G. Caire, R.R. Müller, T. Tanaka, "Iterative Multiuser Joint Decoding: Optimal Power Allocation and Low-Complexity Implementation," *IEEE Transactions on Information Theory*, vol. 50, no. 9, pp. 1950–1973, September 2004.